Magnetic and superconducting behaviour of the R_3Ni (R = La, Pr, Gd, Tb, Ho and Er) systems

1997 J. Phys.: Condens. Matter 9 7419

(http://iopscience.iop.org/0953-8984/9/35/015)

J. Phys.: Condens. Matter **9** (1997) 7419–7434. Printed in the UK PII: S0953-8984(97)79985-5

Magnetic and superconducting behaviour of the R_3Ni (R = La, Pr, Gd, Tb, Ho and Er) systems

C S Garde and J Ray

Low-Temperature Physics Group, Tata Institute of Fundamental Research, Homi Bhabha Road, Bombay 400 005, India

Received 2 December 1996, in final form 4 June 1997

Abstract. Magnetic and transport behaviours of R_3Ni (R = La, Pr, Gd, Tb, Ho and Er) systems have been studied between 2 and 300 K. At low temperatures, all the systems except for R = La exhibit complex magnetic ordering effects. The R = La system exhibits superconductivity. At high temperatures, the transport behaviour has been explained in the framework of the s–d model arising from the interaction between the 3d and the 5d electrons of Ni and R, respectively.

1. Introduction

In recent years, the magnetic behaviour [1] of rare earth (R)–transition metal (X) intermetallic systems has received renewed attention. These systems exhibit complex magnetic and transport behaviour. The magnetic ordering effects in the R–X systems (X = Ni and Co) primarily arise due to interaction [2, 3] of the Ruderman–Kittel–Kasuya–Yosida (RKKY) type amongst the R atoms giving rise to antiferromagnetic (AF) behaviour. With application of external magnetic field H, a ferromagnetic (F) component begins to appear. As H is increased progressively, this F phase is fully developed. These transformations are reflected in steplike increases in the magnetization M measurements. Such complex behaviour has also been observed with the variation of temperature. Above the magnetic ordering temperatures, the s–d scattering process [4] between the X and R atoms may give rise to spin-fluctuation-like effects. These effects are believed to be more pronounced for the X = Ni than X = Co systems as the Ni moment is usually very small ($< 0.1\ \mu_B$). They mainly govern the high-temperature magnetic behaviour and their role has not been investigated in detail in the X = Ni case. In some of these systems, such as R_3Ni, the magnetic ordering transition temperatures have already been determined [5]. The purpose of the present study of R_3Ni (R = La, Pr, Gd, Tb, Ho and Er) systems is to investigate the finer details of the magnetic processes both below and above these transition temperatures and correlate them with the transport behaviour.

2. Experimental details

All the alloys were prepared in an arc furnace under flowing argon conditions. The buttons were flipped and remelted three or four times to ensure homogeneity. These polycrystalline samples were drawn into cylindrical rods by the cold suction technique. Finally they were annealed at 500 °C for 1 week. Our x-ray analyses show that almost all the systems crystallize (table 1) in the orthorhombic structure. They exhibit the usual lanthanide

0953-8984/97/357419+16$19.50

contraction. The annealed and quenched La_3Ni samples crystallize in the hexagonal and orthorhombic phases, respectively. The magnetization M and dc susceptibility χ studies were carried out in a SQUID magnetometer (Quantum Devices, USA). The transport measurements were carried out on the cylindrical rods with approximate dimensions of 25 mm long and about 2 mm in diameter. The standard four-probe method was employed for resistivity ρ measurements. A dc current of 100 mA was passed through the sample using a constant-current source (model 6177C, Hewlett Packard, USA) and the voltage across the sample was measured using a nanovoltmeter (model 181, Keithley Instruments, USA). The accuracy of the ρ measurement is better than 0.01%. For the measurement of thermopower S and thermal conductivity λ, AuFe (0.07% Fe) and Cu thermocouple wires were spot welded at the extremities of the sample rod and the voltages were measured using nanovoltmeters (model 181, Keithley Instruments, USA) to calculate the temperature gradient ΔT. The accuracy of the S and λ measurements is about 5 and 7%, respectively.

Table 1. Crystal parameters for the R_3Ni systems.

System	Crystal structure	a (Å)	b (Å)	c (Å)
Er_3Ni	orthorhombic	6.804 ± 0.001	9.432 ± 0.003	6.245 ± 0.001
Ho_3Ni	orthorhombic	6.852 ± 0.004	9.549 ± 0.006	6.288 ± 0.002
Tb_3Ni	orthorhombic	6.921 ± 0.003	9.605 ± 0.002	6.310 ± 0.001
Gd_3Ni	orthorhombic	6.952 ± 0.003	9.688 ± 0.005	6.367 ± 0.001
Pr_3Ni	orthorhombic	7.182 ± 0.009	9.786 ± 0.006	6.479 ± 0.008
La_3Ni (quenched)	orthorhombic	7.271 ± 0.003	10.243 ± 0.004	6.647 ± 0.003
La_3Ni (annealed)	hexagonal	10.182 ± 0.006	—	6.471 ± 0.005

3. Magnetic behaviour

3.1. Susceptibility studies

The magnetic ordering effects have been investigated using the dc susceptibility χ technique. All the samples were cooled in zero external field. Subsequently, the χ measurements were carried out in an external field of 1 kOe. The sharp cusp (vertical arrow, figure 1) at the critical temperature T_N (table 2) for the R = Er, Ho, Gd and Tb systems indicates that the magnetic ordering is of AF nature. For the R = Ho system, two cusps are exhibited. The first one occurs at $T_N = 18$ K. The second one (at the lower critical temperature $T_R = 9$ K) occurs due to the evolution of another AF structure. Such a change in the magnetic structure in the ordered phase usually arises from the spin-reorientation effect and has been observed [6] in systems such as $NdCu_2$. The cusp at T_R suggests that the structure below T_R is also of the AF type. This is also supported by the M data (section 3.2). Another interesting feature observed (for $T < T_N$) is the manifestation of thermal hysteresis effects. The hysteresis behaviour indicates that the two magnetic phases coexist [7] over a finite temperature range due to superheating and supercooling effects. This is a characteristic feature of a first-order transition involving latent heat of transformation. For R = Gd, the value of χ is found to increase for $T < T_N$. This indicates that the AF ordering is of complex nature and could coexist with an F component. The value of T_N, for all the systems except R = Ho, is found to be quite close to the earlier reported [5, 8] values. In the case of Ho, the earlier reported value of T_N is larger than our value ($\sim$18 K) by about 20 K. The reason for this difference is not clear.

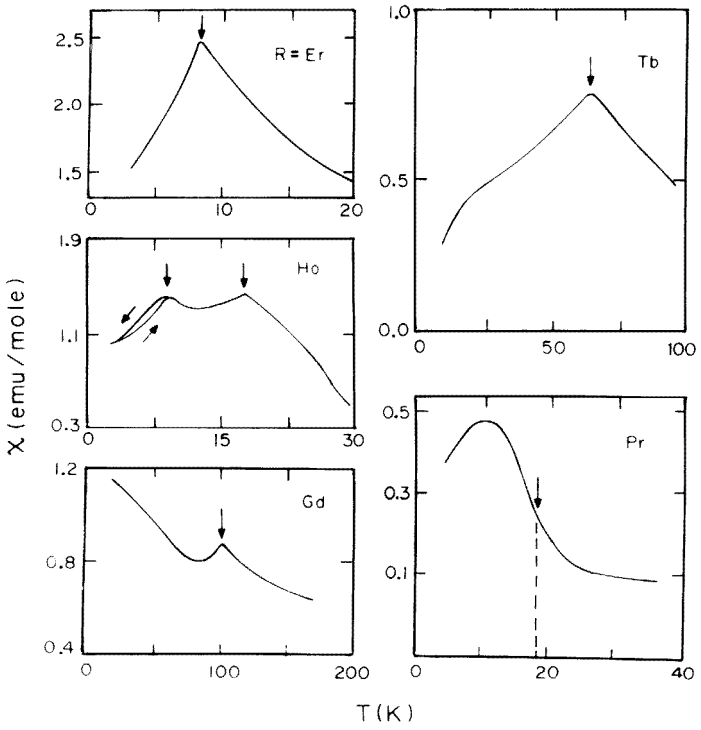

Figure 1. χ versus T curves.

Table 2. Various characteristic temperature scales for the R_3Ni systems.

System	T_N (K)	T_R (K)	T_C (K)	H_m (kOe)	M (55 kOe) (μ_B/R)	$g_J J$ (μ_B/R)
Er_3Ni	9	—	—	7	5.8	9.0
Ho_3Ni	18	9	—	13	5.4	10.0
Tb_3Ni	62	—	—	40	4.5	9.0
Gd_3Ni	100	—	—	19	3.9	7.0
Pr_3Ni	—	—	18	—	0.7	3.2

For the R = Pr system, the χ curve exhibits a sudden increase (figure 1) below 25 K. This indicates the onset of ferromagnetic or ferrimagnetic (F) order. The transition temperature $T_C = 18$ K (table 2) is identified with the point of inflection (vertical arrow, figure 1). At still lower temperatures ($T < 10$ K), the curve exhibits (figure 1) a broad maximum instead of a sharp cusp. This transition is therefore not likely to be due to AF order. Instead it arises due to the usual domain wall movement effects [5, 9] observed in F systems. For $T < T_C$, the following two competing effects occur. Firstly, the thermal disorder in the spin system decreases (with lowering of temperature) and consequently χ increases. Secondly, the movement of the domain walls also slows down, which, on the other hand, decreases χ. These two competing processes [5, 9] thus give rise to the observed maximum in the χ curve.

The behaviour of the effective magnetic moment μ_{eff} associated with the R atoms in the R_3Ni systems is now analysed. In the molecular field approximation we obtain $\mu_{eff}^2 = 3k_B\chi T/N_A$, where k_B and N_A are the Boltzmann constant and Avogadro number, respectively. The free ion moment (Hund's limit) value is given by $\mu_0 = g_J(J(J+1))^{1/2}$, where g_J is the Lande factor and J is the total angular moment. Using the above formula, the temperature dependence of μ_{eff} is found to exhibit complex behaviour (figure 2). We find (figure 2) that, in most cases, $\mu_{eff} > \mu_0$ in the paramagnetic regime ($T > T_N$ or T_C). The value of μ_0^2 is indicated by the dashed line (figure 2). For R = Er, $\mu_{eff} < \mu_0$ for $T > 150$ K, whereas for R = Ho, $\mu_{eff} = \mu_0$ for $T > 100$ K. We note that for R = La, $\mu_{eff} \neq 0$ even though La does not possess any 4f electrons (hence $\mu_0 = 0$). Thus these departures of μ_{eff} from the μ_0 values suggest formation of induced magnetic moment on the R atom, probably arising due to spin fluctuation (SF) effects from the Ni 3d band. Such induced moment effects have been attributed [10], in the case of non-magnetic Y_3Ni as well as magnetic Gd_3Ni, to the hybridization of the 3d electrons of Ni and 5d electrons of the R. We also note that crystal field (CF) effects cannot account for the inequality $\mu_{eff} > \mu_0$ in these systems. If the overall CF splitting is denoted by Δ, then for $T > \Delta$ both the CF levels will be equally populated and we shall have $\mu_{eff} = \mu_0$ [11], whereas for $T < \Delta$ the excited CF level will only be partially populated and this would result in $\mu_{eff} < \mu_0$ [11]. Further, on the basis of CF effects, μ_{eff} will decrease monotonically [11] with lowering of temperature. However, on the contrary, our data show that in many cases such a decrease is not observed and the reverse trend ($\mu_{eff} > \mu_0$) occurs for most of the systems. This also suggests that the CF effects in these systems are not important and the departure of μ_{eff} from the μ_0 value may arise due to SF contribution from the Ni band affecting the 5d band of the R atom.

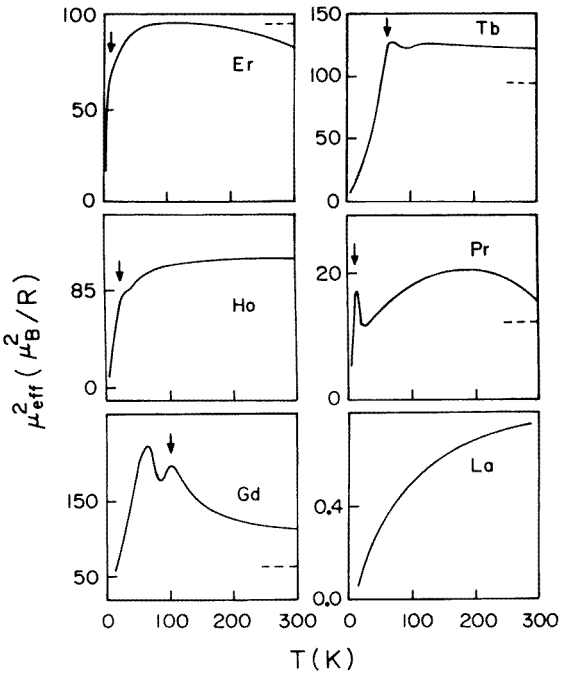

Figure 2. μ_{eff}^2 versus T curves.

For $T < T_N$ or T_C, μ_{eff} shows a change in slope or a maximum (vertical arrow, figure 2). For R = Gd, the second maximum (figure 2) at the lower temperature could arise due to the increase in χ as the temperature is gradually lowered below T_N.

3.2. Magnetization studies: field dependent effects

The M behaviour (for $T < T_N$) is discussed. The M curves at 5 K for R = Er, Ho, Gd and Tb exhibit a linear increase up to a value H_m (vertical arrow, figure 3). H_m (table 2) is found to vary between 7 and 40 kOe. This linear dependence corresponds to the usual behaviour [3] observed for a typical AF system. However, for $H > H_m$, M increases faster than the initial linear variation. This increase suggests that the system evolves to a new magnetic structure with more and more spins aligned in the direction of the field H. This process is reminiscent [12] of metamagnetic behaviour as observed in systems such as ErAg. The increase in the M value can arise either due to gradual flip of spins or due to abrupt flip of a large number of spins. Both these effects are observed in our systems. For the R = Er, Ho and Gd systems the M value increases gradually for $H > H_m$, whereas for R = Tb the M value exhibits an abrupt increase for $H > H_m$. Therefore, for the former case (R = Er, Ho and Gd) the alignment process occurs gradually up to the highest applied field (H = 55 kOe), whereas for the latter case (R = Tb), even at lower fields (H = 45 kOe), the M curve shows strong saturation effects. In both the cases, the free ion value (table 2) for the magnetic atom is not reached at the highest field of 55 kOe.

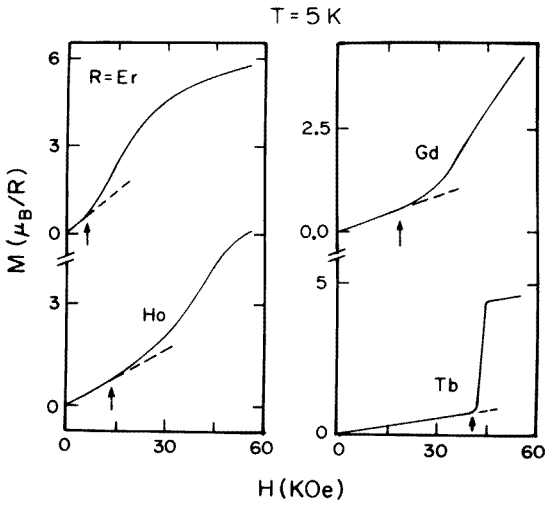

Figure 3. M versus H curves at $T = 5$ K.

Of the above four systems which exhibit metamagnetic behaviour, only the R = Tb system exhibits (figure 4) complex hysteresis behaviour as explained below. For the R = Tb system, the M curve rises rapidly at H_m (vertical arrow, figure 4). The M curve decreases linearly as H is decreased below H_m ($\sim$40 kOe), indicated by the vertical arrow (figure 4). With further decrease of H value, M exhibits a drop (indicated by the dashed ellipse, figure 4) around $H = 4$ kOe and a plateau occurs (inset of figure 4) around $H = -2$ kOe. The corresponding value of M at this plateau is about 2.3 μ_B/Tb which is only half the value (table 2) of M at $H = 55$ kOe. Such fine structure in the M curve indicates that

more than one magnetic ordered state is present. As the H value becomes progressively negative, M drops further from the plateau value (inset, figure 4) and eventually exhibits a linear dependence (at $H \sim -5$ kOe) indicating that the system has reverted back to the normal AF order. Finally, the M curve drops again (at $H \sim -H_m$) and reaches a saturation value at -55 kOe. During the reverse cycle (increasing the field from -55 kOe to 55 kOe) the M curve is completely symmetric with respect to that obtained by decreasing H (from 55 kOe to -55 kOe).

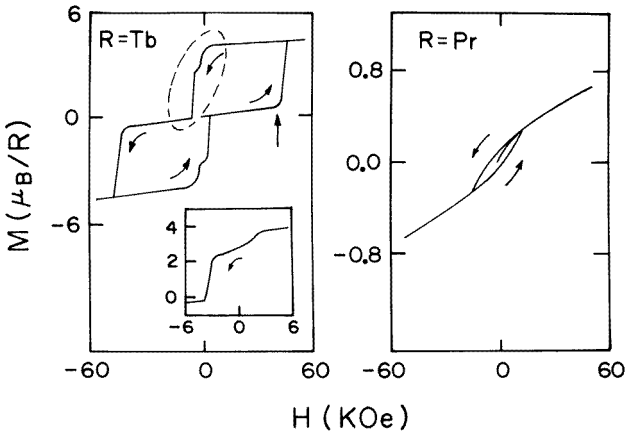

Figure 4. M versus H curves for the R = Tb and Pr systems. The inset shows, in an expanded scale, the portion of the curve (for R = Tb) indicated by the dashed ellipse.

For the R = Pr system, the M curve exhibits (figure 4) the usual hysteresis behaviour typical of a ferromagnet. Even for this system the free ion limit is not reached (table 2) at the highest field of 55 kOe.

We now discuss the M behaviour for $T > T_N$. The M curves (figure 5) for R = Ho, Gd and Tb for $T > T_N$ exhibit the usual linear behaviour due to paramagnetic effects. However, for R = Er, a clear decrease from the linear behaviour (even for $T > T_N$) is observed (for $H > 30$ kOe, figure 5). Such a behaviour has been also observed [13] in other systems such as TmCu and has been attributed to the influence of CF effects. The presence of short-range magnetic correlation effects above T_N could also be responsible for such effects. Neutron studies can be usefully employed to distinguish between these two possibilities.

4. Superconductivity behaviour

4.1. Susceptibility and resistivity studies

Of all the systems studied, only the R = La system was known [14–16] to exhibit superconductivity. These recent studies indicated complex superconducting behaviour depending on atomic disorder present in the alloy as well as the possibility of a novel pairing mechanism. In view of this, we have carried out detailed transport and magnetic studies on different heat treated samples. The χ curves (figure 6) for the quenched and annealed samples are quite different. All the samples were cooled in zero external field. Subsequently, the χ measurements were carried out in an external field of 100 Oe.

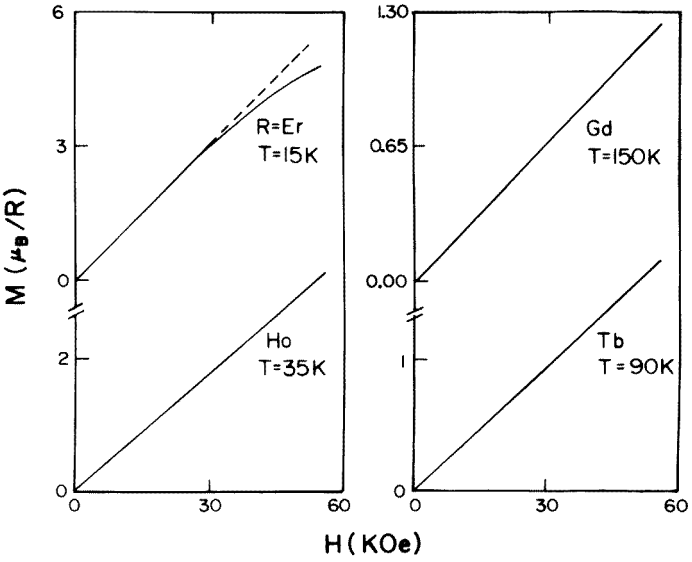

Figure 5. M versus H curves for $T > T_N$.

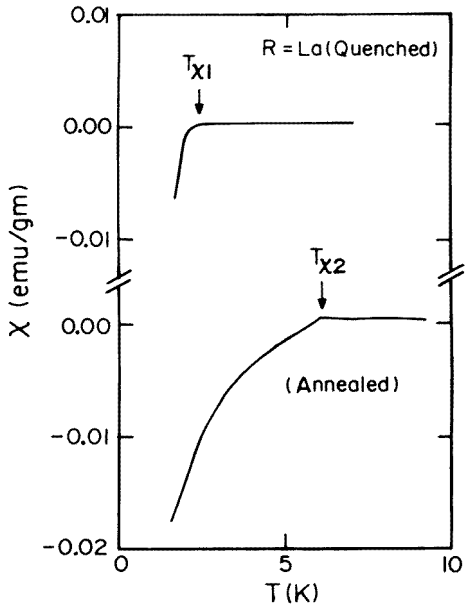

Figure 6. χ versus T curves for the R = La system.

For the quenched samples, the onset of the diamagnetic (negative) signal (figure 6) occurs below the characteristic temperature $T_{\chi 1} = 2.4$ K (table 3). For the annealed sample the diamagnetic signal appears at the higher temperature $T_{\chi 2} = 6.1$ K. However this transition is broader compared to that observed at $T_{\chi 1}$. For $T < T_{\chi 2}(= 6.1$ K), the signal continuously increases down to 1.8 K, indicating that a greater portion of the sample

volume progressively participates in the superconducting behaviour. The manifestation of two distinct onset temperatures (table 3) is most probably related to the fact that the crystal structures for these two different heat treated samples are different. The quenched and annealed samples exhibit orthorhombic and hexagonal structures, respectively, as analysed from our x-ray data. At the lowest temperature ($T = 1.8$ K), the magnetization signal for both the annealed and the quenched samples was found to correspond to about 70% of the total shielding signal of an ideal superconductor. We note that the diamagnetic signal was not found to be temperature independent down to $T = 1.8$ K. This would indicate that the bulk superconducting transition temperature may have a value less than 1.8 K.

Table 3. Superconducting characteristic temperature scales for the R = La system.

System	$T_{\chi 1}$ (K)	$T_{\chi 2}$ (K)	$T_{\rho 1}$ (K)	$T_{\rho 2}$ (K)
La_3Ni (quenched)	2.4	—	2.2	—
La_3Ni (annealed)	—	6.1	—	6.1

The resistivity ρ data also support the χ data. For the quenched samples, the ρ curve drops (figure 7) precipitously and finally becomes zero at $T_{\rho 1} = 2.2$ K. For the annealed samples, the corresponding ρ curve (figure 7) goes to zero at $T_{\rho 2} = 6.1$ K. In both cases the zero-resistivity characteristic temperatures $T_{\rho 1}$ and $T_{\rho 2}$ are close (table 3) to the superconducting onset temperatures $T_{\chi 1}$ and $T_{\chi 2}$, respectively. The vanishing of the ρ value at $T_{\rho 1}$ and $T_{\rho 2}$ indicates that the onset of superconductivity occurs at two distinctly different temperatures and the superconducting behaviours are strongly influenced by the crystal structure of these samples.

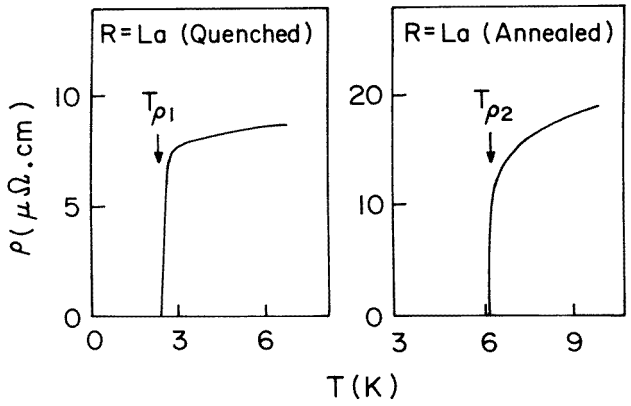

Figure 7. ρ versus T curves for the R = La system.

5. Transport studies

5.1. Resistivity behaviour

5.1.1. Low-temperature effects ($T \leqslant T_N$). The ρ curves for all the systems exhibit complex behaviour. For R = Er and Ho, the ρ curve exhibits (figure 8) a minimum ρ_{min} at $T_{m1} = 9$ and 20 K, followed by a maximum ρ_{max} at $T_{M1} = 6$ and 12 K, respectively. The value of

T_{m1} is found to be close (tables 2 and 4) to that for T_N for both the systems. The increase in the ρ curve (for $T < T_{m1}$) could be due to the formation of an energy gap [11] in the density of states (DOS) near the Fermi energy E_F due to AF ordering. Such a gap formation has been observed [11] in the elemental systems Ho and Dy also. Further, due to the ordering of the magnetic moments (for $T < T_N$) the contribution from the spin disorder resistivity term decreases. Thus the above two competing processes give rise to a broad maximum ρ_{max} at lower temperatures. This broad peak is a characteristic signature for such AF systems and has been observed for elemental Ho and Dy as well as for our R = Ho system. However for R = Er, the maximum is quite sharp and therefore the above mechanism may not be valid in this case. The possibility of spin-reorientation-like effects giving rise to this feature needs to be further investigated. For R = Ho, apart from the occurrence of this maximum, thermal hysteresis effects are also observed for $T < T_{M1}$. This could arise from spin reorientation effects as discussed earlier (section 3.1). For R = Gd, the ρ curve exhibits (figure 8) a change in slope at $T_1 = 100$ K and then drops monotonically down to 2 K. The value of T_1 is found to be close (tables 2 and 4) to T_N. For R = Tb, the ρ curve exhibits a minimum at $T_{m1} = 100$ K followed by a maximum at $T_{M1} = 55$ K. The value of T_{M1} is found to be quite close (tables 2 and 4) to that for T_N. The R = Pr system exhibits a change in slope near $T_1 = 12$ K. This value is much lower (tables 2 and 4) than that of T_C ($\sim$18 K). We note that the large values of $\rho(0)$ as $T \to 0$ (figure 8) in some of the systems may be due to microscopic cracks and inhomogeneities present in spite of the samples being subjected to an annealing treatment.

Table 4. Characteristic temperature scales deduced from the ρ and S curves.

	ρ data			S data	
System	T_{m1} (K)	T_{M1} (K)	T_1 (K)	T_{m2} (K)	T_{M2} (K)
Er_3Ni	9	6	—	—	7
Ho_3Ni	20	12	—	18	13
Tb_3Ni	100	55	—	55	45
Gd_3Ni	—	—	100	100	90
Pr_3Ni	—	—	12	8	12

5.1.2. High-temperature behaviour ($T > T_N$). For $T \geqslant 20$ K, the ρ curves except for R = Tb begin to develop (figure 9) a strong temperature dependence and the value of ρ increases monotonically. A change of sign in the curvature of the ρ curve occurs in this region ($T \sim 50$ K). At still higher temperatures ($T \geqslant 200$ K), all the ρ curves (figure 9) exhibit a pronounced tendency to saturate.

In principle, this ρ behaviour could arise due to SF [17] or CF [18] effects. However, we have shown earlier (section 3.1) that SF effects are most likely to be present in these systems. Hence we have analysed the ρ behaviour in the framework of SF effects. We also note that CF effects may not be responsible for the ρ behaviour for the following reason. For the R = La system (with zero 4f occupancy number), the CF effects would be zero, whereas the ρ behaviour of the R = La system is similar (figure 9) to those for the other R systems having a finite f occupancy number. This implies that the ρ behaviour in the R_3Ni systems is not due to CF effects, although other systems such as RIn_3 have been analysed [18] on the basis of CF effects to explain similar ρ behaviour.

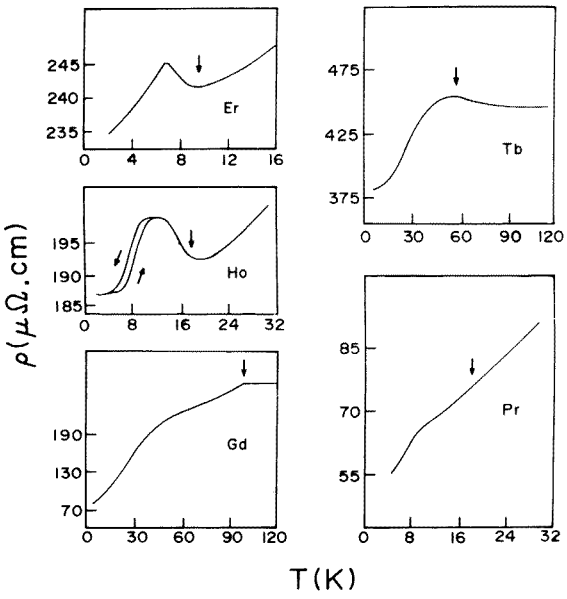

Figure 8. ρ versus T curves. The vertical arrows indicate the magnetic ordering temperatures detected from our χ studies.

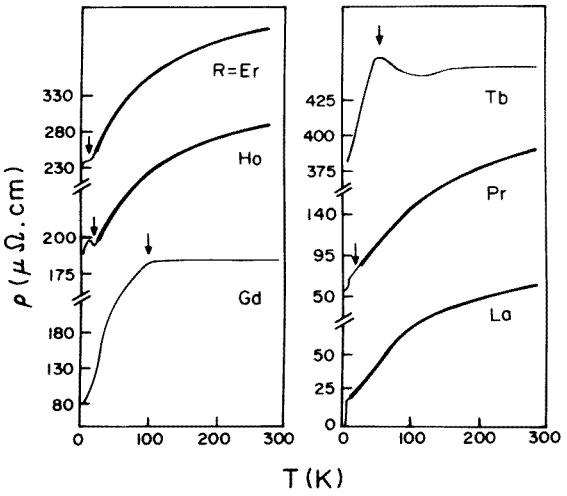

Figure 9. ρ versus T curves. The thickened portion of the curve indicates the temperature range over which the fitting was carried out. The vertical arrows indicate the magnetic ordering temperatures detected from our χ studies.

The ρ contribution arising from the SF effects could be understood as follows. The interaction of the 5d band (of the R atom) with the 3d band (of the Ni atom) can lead to a partial depopulation of the 5d band. This may result in formation of a hybridized band near the Fermi energy E_F. As a consequence of this hybridization, additional scattering states become available and give rise to a strong temperature dependent contribution to ρ.

This scattering process gives rise to an increase of ρ for $T > 20$ K. If the width of the hybridized band is $k_B T_0$ then the temperature dependence of ρ in this s–d model can be expressed [17] as

$$\rho = \rho_0 + a_0 T + b_0 \exp(-T_0/T) \tag{1}$$

where ρ_0 is the residual resistivity and a_0 and b_0 are the strengths of the electron–phonon scattering and s–d scattering contributions, respectively. a_0 depends on both the electronic and the phononic density of states, whereas b_0 is proportional only to the electronic density of states N. The linear term ($= a_0 T$) is the usual electron–phonon contribution. The exponential term represents the s–d scattering and could possibly give rise to SF effects as observed in systems [17] such as Y_9Co_7. This s–d scattering process is best observed when the spin disordered contribution is dominant for $T > T_N$. Equation (1) has thus been fitted to the experimental data (for $T > T_N$) using the least-squares method with ρ_0, a_0, b_0 and T_0 chosen as the free parameters. For R = Er, Ho, Pr and La systems, the agreement (figure 9) of the fitted curve with the experimental data is satisfactory. The rising part ($T > 20$ K) of the ρ curve is matched by adjusting the coefficient b_0 of the exponential term. We note that for the above four systems the value of T_N is small ($T_N < 20$ K) and the rising part of the ρ curve (for $T > 20$ K) corresponds to the paramagnetic phase and can be suitably accounted for by the exponential term in (1), whereas for R = Gd and Tb the value of T_N itself is large (∼100 K) and hence the rising part of the ρ curve is influenced by the interactions of the magnetically ordered phase. In such situations the rising part of the ρ curve cannot be estimated using (1). Hence no attempt was made to carry out the fitting for the R = Gd and Tb systems.

Table 5. Parameters obtained from the fitting procedure.

System	ρ_0 ($\mu\Omega$ cm)	a_0 ($\mu\Omega$ cm K^{-1})	b_0 ($\mu\Omega$ cm)	T_0 (K)	A ($\times 10^{-2}$ μV K^{-2})	B (μV K^{-1})
Er_3Ni	241	0.15	199	59	3.3	−3.4
Ho_3Ni	180	0.07	149	65	1.9	1.8
Tb_3Ni	—	—	—	—	1.6	−1.2
Gd_3Ni	—	—	—	—	1.4	0.6
Pr_3Ni	62	0.18	124	62	0.4	−0.2
La_3Ni(A)	19	0.05	75	55	0.3	−0.2
Y_9Co_7 [17]	7	0.09	173	104	−1.6	−8.0

It is of interest to note that the value of T_0 (table 5) is found to be nearly the same (55–65 K) for all the systems irrespective of the f-electron number of the R atom. This suggests that the interaction of the 5d band electrons (of the R atom) with the conduction electrons is mainly responsible for the s–d scattering effects. The values of a_0, b_0 and T_0 are found to be comparable (table 5) to the values reported [17] for a typical SF system such as Y_9Co_7. Further, the value of b_0 is found to decrease as the f-electron number is varied as R changes from R = Er to La. As b_0 is proportional to the DOS, this implies that N decreases also in the same sequential manner as R is varied from Er to La. The implication of this variation of N is discussed later (section 5.2.2). The value of ρ_0 (table 5) has been obtained by fitting the data for the temperature range $T > T_N$. For $T < T_N$, the ρ value drops sharply (figure 8) and $\rho(0)$ is the extrapolated value in the limit of $T \to 0$. For this reason, the value of ρ_0 is different from $\rho(0)$.

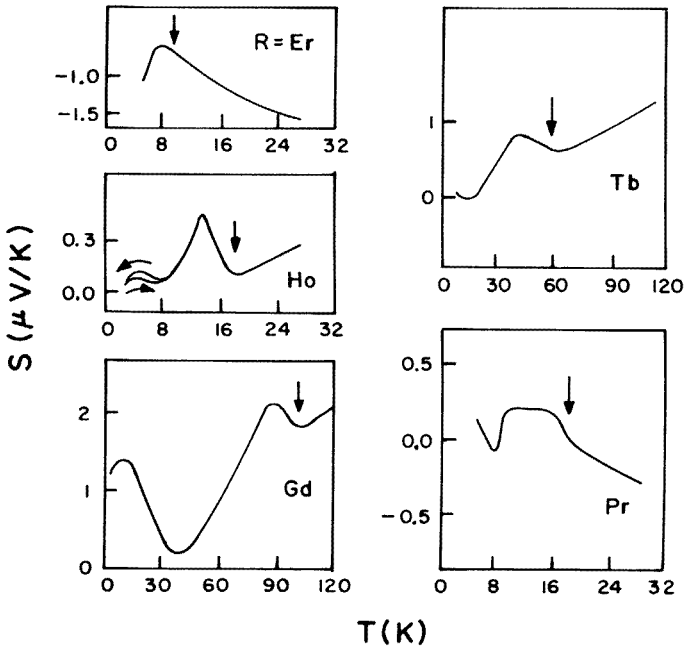

Figure 10. *S* versus *T* curves. The vertical arrows indicate the magnetic ordering temperatures detected from our χ studies.

5.2. Thermopower behaviour

5.2.1. Low-temperature features. The thermopower S is found to show complex behaviour (figure 10) near T_N and T_C. No definite signature at the ordering temperature has been observed in the S data. For R = Er, a maximum is found to occur (figure 10) at $T_{M2}(= 7$ K), just below $T_N(= 9$ K), whereas for R = Ho, Gd and Tb a minimum is found to occur (figure 10) at T_{m2} (table 4), quite close to the value (table 2) of the respective T_N. For R = Ho, a thermal hysteresis effect is observed below 8 K ($\sim T_R$) similar to the ones observed in the χ and ρ curves. The S curve for R = Pr exhibits a change in slope at T_C. The extremum features below T_N and T_C could arise due to electron–magnon scattering [4] in the ordered state.

5.2.2. High-temperature features. The S behaviour (figure 11) of these systems for $T \geqslant T_N(=$ 10–100 K) is found to be complex. At higher temperatures ($T >$ 200 K), it is found to vary linearly. This linear behaviour can be fitted (figure 11) by the following equation:

$$S = AT + B. \tag{2}$$

The first term (AT) denotes the usual Mott term in the free electron approximation and is proportional to the energy derivative of density of states N at E_F. The second term (B) is a temperature independent term and its value is given by the intercept (figure 11) on the S axis of the extrapolated straight line at $T = 0$ K. Both these terms can arise from the complex s–d scattering process (see section 5.1.2). The sign of A is found to be positive (table 5) for all the systems, whereas the value of B is found (table 5) to be positive for R = Gd and

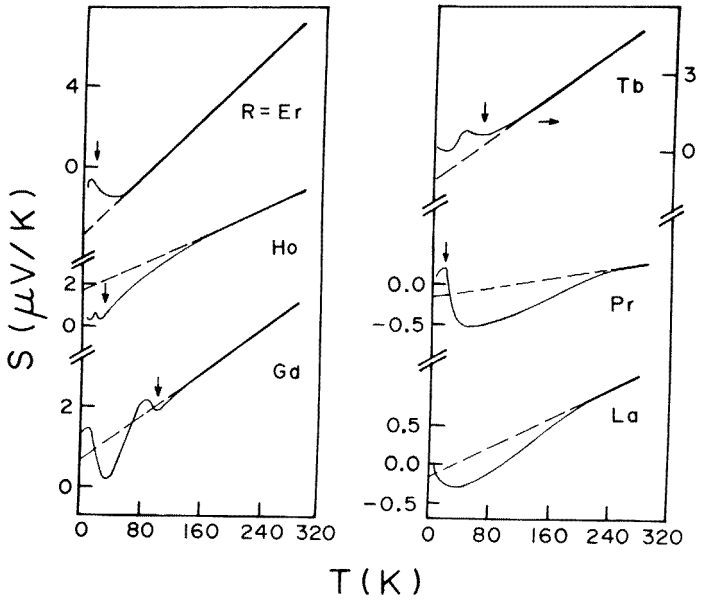

Figure 11. S versus T curves. The vertical arrows indicate the magnetic ordering temperatures detected from our χ studies. The horizontal arrow refers to the appropriate S axis for the R = Tb system.

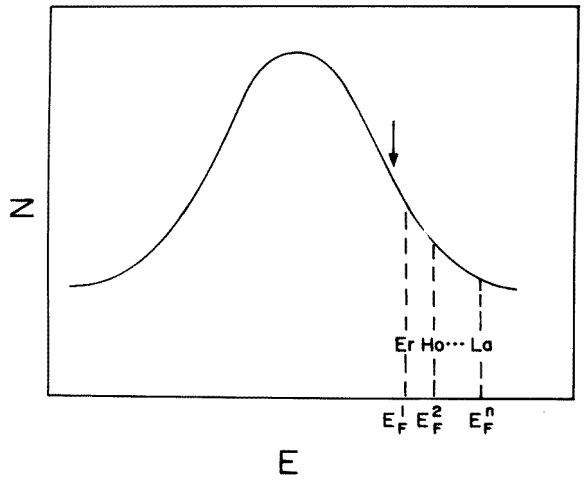

Figure 12. A schematic diagram of the density of states N (of the hybridized band) versus electron energy E. E_F^1, E_F^2, ..., E_F^n are the values of the Fermi energy for Er, Ho, ..., La, respectively.

Ho and negative for all other systems. As A is proportional to $-\partial N/\partial E$ (at E_F), E_F itself will lie on the right-hand side of the peak (where $\partial N/\partial E < 0$) in the N curve (figure 12) of the hybridized band shown schematically. Further, the fitted value of A decreases (table 5) as the R atom is varied from Er to La. This implies that the value of the slope $\partial N/\partial E$ also

must decrease. Hence E_F will increasingly move from a region of larger to a smaller value of the slope. Moreover the value of N (as deduced from the ρ behaviour—section 5.1.2) also decreases with the same sequential variation of the R atom. This implies that E_F will be located in the region to the right of the inflection point (indicated by the arrow). In this region the value of the slope decreases after passing through a maximum at the inflection point.

5.3. Thermal conductivity behaviour

The thermal conductivity λ curves (figure 13) for all the systems (except R = Gd) exhibit a monotonic variation from 2 to 300 K. No anomaly has been detected in the λ curves near T_N and T_C for these systems. For R = Gd only, the curve shows (figure 13) a shallow minimum near T_N.

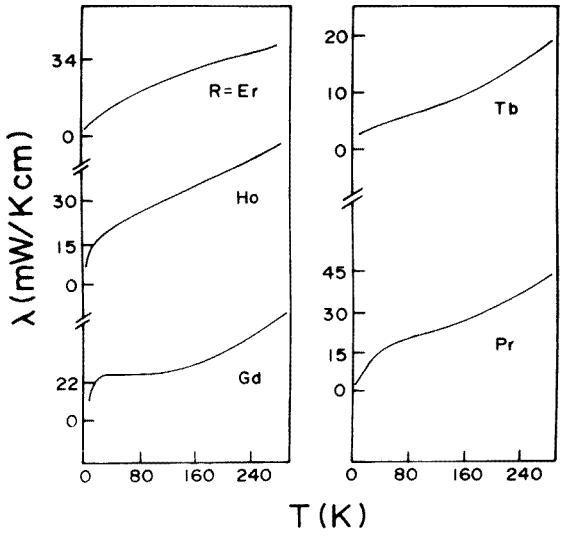

Figure 13. λ versus T curves.

The λ behaviour arises [19] due to the combined influence of electronic λ_e, phononic λ_p and magnetic λ_m terms. Therefore the total λ at a given temperature is given by $\lambda(T) = \lambda_e(T)+\lambda_p(T)+\lambda_m(T)$. The result of interplay of the above three terms is reflected (figure 14) in the temperature dependence of the Lorenz number $L = \rho(T)\lambda(T)/T$. In the free electron picture, L arises only from the λ_e term and becomes temperature independent. Its value is given by $L_0 = 2.45 \times 10^{-8}$ W Ω K^{-2}. Our λ data reveal that L is temperature dependent and therefore the free electron picture is not valid for our systems. The value of L at 10 K is found (figure 14) to be about five times larger than L_0. For R = Er, Ho and Pr the value of L/L_0 is found to show (figure 14) a maximum at a temperature close to T_N, whereas for R = Gd and Tb it shows a change in slope near T_N. Hence no definite signature near the magnetic transition temperature has been observed in the L/L_0 curve. For all the systems, L/L_0 shows a rapid decrease (figure 14) as the temperature is increased beyond 50 K. This occurs due to a decrease [19] in λ_p as the phonon–phonon anharmonic interaction increases around this temperature. Only at high temperature ($T > 100$ K) does L/L_0 become almost temperature independent. Even this high temperature value is found

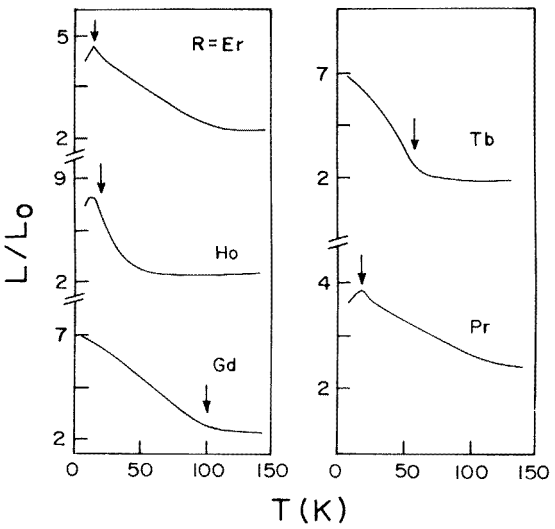

Figure 14. L/L_0 versus T curves. The vertical arrows indicate the magnetic ordering temperatures detected from our χ studies.

to be about twice the free electron value L_0. Such a deviation from L_0 indicates that contributions from λ_p are important and may be comparable to λ_e.

6. Conclusions

The R_3Ni systems are thus found to exhibit complex magnetic order of the AF type for R = Gd, Tb, Ho and Er and of the F type for R = Pr. For R = Ho, conversion from one AF type to another AF type occurs possibly due to spin reorientation effects. For R = Pr, domain wall effects within the F state below T_C are likely to be present. For R = Gd, Tb, Ho and Er systems, a spin alignment process of metamagnetic type has been observed. For R = Tb, complex field reversal effects have been observed. The ρ and S behaviours have been analysed in the framework of the s–d model. The characteristic temperature T_0 is found to be independent of the R atom. This suggests that these s–d scattering effects arise from the 5d electrons of the R atoms and the role of f electrons in the transport properties of these systems is negligible. The position of E_F with variation of R atom has also been analysed. For the R = La system, superconducting behaviour was found to be sensitive to its crystal structure.

Acknowledgments

We thank A Chinchure for useful discussions on crystal field effects in these systems and K V Gopalkrishnan for his help in carrying out the SQUID based measurements.

References

[1] Franse J J M and de Boer F R 1995 *J. Magn. Magn. Mater.* **140–144** 789 and references therein
[2] Date M 1990 *J. Magn. Magn. Mater.* **90/91** 1
Date M 1988 *J. Phys. Soc. Japan* **57** 3682

[3] Gignoux D and Schmitt D 1995 *J. Alloys Compounds* **225** 423
[4] Gratz E and Zukermann M J 1982 *Handbook on the Physics and Chemistry of Rare Earths* ed K A Gschneidner Jr and L Eyring (Amsterdam: North-Holland) p 117
[5] Buschow K H J 1980 *Ferromagnetic Materials* vol 1, ed P Wohlfarth (Amsterdam: North-Holland) p 297
[6] Gratz E, Loewenhaupt M, Divis M, Steiner W, Bauer E, Pillmayr N, Muller H, Nowotny H and Frickk B 1991 *J. Phys.: Condens. Matter* **3** 9297
[7] Rao C N R and Rao K R 1978 *Phase Transitions in Solids: an Approach to the Study of the Chemistry and Physics of Solids* (New York: McGraw-Hill)
[8] Talik E 1994 *Physica* B **193** 213
[9] Kaczorowski D, Noel H, Potel M and Zygmunt A 1994 *J. Phys. Chem. Solids* **55** 1363
[10] Talik E and Neumann M 1994 *Physica* B **193** 207
[11] Taylor K N R and Darby M I 1972 *Physics of Rare Earth Solids* (London: Chapman and Hall) p 53
[12] Kaneko T, Abe S, Sakurada S, Yoshida H, Kido G and Nakagawa Y 1992 *J. Magn. Magn. Mater.* **104–107** 1401
[13] Morin P and Schmitt D 1990 *Ferromagnetic Materials* vol 5 ed K H J Buschow and E P Wohlfarth (Amsterdam: Elsevier) p 1
[14] Garde C S, Ray J and Chandra G 1993 *J. Alloys Compounds* **198** 165
[15] Sato N, Imamura K, Sakon T, Komatsubara T, Umehara I and Sato K 1994 *J. Phys. Soc. Japan* **63** 2061
[16] Sato N, Koga N, Imamura K, Sakon T and Komatsubura T 1995 *Physica* B **206/207** 565
[17] Sarkissian B V B 1986 *J. Phys. F: Met. Phys.* **16** 755
[18] Kletowski Z 1993 *J. Phys.: Condens. Matter* **5** 8955
[19] Ziman M 1960 *Electrons and Phonons* (London: Oxford University Press) p 385